

Electromagnetic Antenna based on Transmitter-Receiver Crossing Coil

*Jun Zhang, **Yangcheng Xu, ***Yunbo Li, ****Fenghao Yang, *****Yanqing Wu

*Chongqing Research Institute of China Coal Technology & Engineering Group Corporation,
Chongqing 400039, China; School of Geosciences and Info-physics, Central South University
Changsha 410083, China

**Chongqing Research Institute of China Coal Technology & Engineering Group Corporation
Chongqing 400039, China (Corresponding author: xuyangcheng1983@163.com)

***Chongqing Research Institute of China Coal Technology & Engineering Group Corporation
Chongqing 400039, China

****Department of Mathematics and Statistics, York University
Toronto M3J1P3, Canada

*****Chongqing Research Institute of China Coal Technology & Engineering Group
Corporation

Chongqing 400039, China

School of Geosciences and Info-physics, Central South University
Changsha 410083, China

Abstract

The small multiturn overlapping coil is always used in mine transient electromagnetic exploration. For the effect of turn-off, the first field dominates total field during the off-time of transmitting current and early after off-time. This may cause unresponsive for shallow low resistance anomaly. So we suggest that use cross coil for first field eliminating: Analyzes the distribution of first field inside and outside the transmitting coil during the off-time; Deduces the analytic expression of magnetic flow for first field inside the receiving coil; Worked out the coefficient of position for receiving coil is 0.93 when the magnetic flow for first field inside the receiving coil is 0. According to laboratory experiment for low resistance model and site detecting

for tunnel filled with water, we verify the availability of cross coil for first field eliminating and low resistance anomaly detecting. It provides technical support to mine transient electromagnetic exploration.

Key words

Mine transient electromagnetic, Antenna, First field eliminating, Transmit-receive crossing coil.

1. Introduction

Sensitive to water, the transient electromagnetic method is widely used in detecting hidden water disasters in coal mines. As the intensity of emission currents and roadway size are subject to conditions, it is a common way to increase the transmitter moment by means of multi-turn loop in detecting deep strata ahead. The shut-off of emission current needs time. Therefore, there will be a large primary field in the receiving loop from the beginning of the shut-off to a short time after the end of the shut-off, incurring current clipping in the receiver; meanwhile, the primary field is superimposed on the secondary field and dominates the total field, which strengthens the total field. As a result, the response to low resistivity anomaly in shallow strata is sluggish, and the detection effect is weakened.

The primary field will interfere with transient electromagnetic detection no matter on the ground, in the air or in the coal mine. The following approaches are the main means to eliminate the influence of the primary field [1-2]: Bai and Ji excluded the primary field from the total field in the shut-off period [3-5]; Liu et al. detected the coal mine information in shallow strata by reducing the size and turns of coils [6]; in counteracting the primary field, the concentric compensation technology was adopted by the AeroTEM system and the Helicopter Time-Domain Electromagnetic (HTEM) system in Jilin University [7-9]. Although these methods have achieved some results, underground detection is still problematic: the prerequisite of excluding primary field is to take detailed records of the waveform of emission current and to check the coupling coefficient between the transmitting coil and the receiving coil, which is difficult at current technologic levels; the means of reducing coil size and turn cannot balance the needs of shallow detection and deep detection; the concentric compensation technology suits for central loop with fixed antenna and magnetic probe that receives signals, but is unsuitable for the overlapping loop which is easy to carry and which requires frequent assembly and disassembly.

Therefore, in order to successfully eliminate the influence of the primary field in downhole transient electromagnetic detection, the receiving antenna and transmitting antenna are arranged staggered in this paper. An analysis is conducted on the distribution of the primary field in and out of the transmitting coil during the time when the transmitting current is shut off; the analytical expression of the magnetic flux in the primary field is deduced in the interior of the receiving antenna; then, we calculate the transmitting and receiving range when the magnetic flux is 0. Through the indoor test of the low resistivity model and the on-spot detection of the water-enriched roadway, we verify the effectiveness of the staggered antennas in eliminating the influence of the primary field and probing low resistivity anomaly, providing technical support for the underground transient electromagnetic detection.

2. Principle

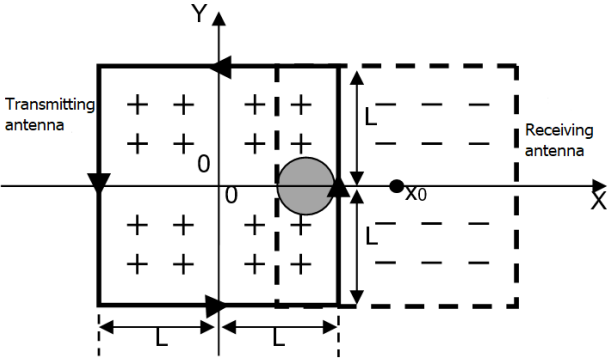


Fig.1. Schematic Diagram of the Receiving Antenna

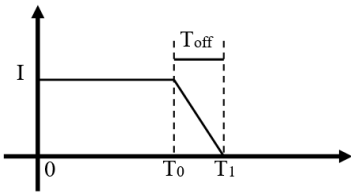


Fig.2. Schematic Diagram of the Transmitting Current

The direction and waveform of the transmitting current are shown in Figure 1 and Figure 2 [10]-[12], respectively. Under the effect of the inductance and the capacity of the transmitting antenna, the transmitting current cannot be shut off immediately. During the shut-off period, according to the right-hand rule, the direction of the inner magnetic field is positive while the direction of the outer magnetic field is negative. When using overlapping loops, the receiving antenna and the transmitting antenna are concentric and equal in size. Therefore, the inner primary

magnetic field is positive. It is superimposed on the secondary field and dominates the total field, which strengthens the total field. As a result, the apparent resistivity mutates in shallow strata, weakening the detection effect.

When using the transient electromagnetic technology to detect the underground coal mine, the staggered arrangement of receiving antenna is shown in the dotted box in Figure 1. As the receiving antenna is non-concentric with the transmitting antenna, the positive and negative inner primary magnetic fields coexist in the shut-off period. If the transmitting and receiving range is proper, the positive and negative fields will counteract each other. Accordingly, the primary magnetic flux is 0 and there will be no more primary field effect caused by current shut-off.

3. Determining the Positions of the Receiving and Transmitting Antennas

According to the literature 1, the primary magnetic field $BF_1(t)$ of the transmitting antenna at the moment t is:

$$\begin{aligned}
 & E_{z_1}(t) \\
 &= \frac{\mu_0 I(t)(L+y)}{4\pi(L+y)^2+z^2} \left(\frac{L+x}{\sqrt{(L+x)^2+(L+y)^2+z^2}} + \frac{L-x}{\sqrt{(L-x)^2+(L+y)^2+z^2}} \right) \\
 &+ \frac{\mu_0 I(t)(L-y)}{4\pi(L-y)^2+z^2} \left(\frac{L-x}{\sqrt{(L-x)^2+(L-y)^2+z^2}} + \frac{L+x}{\sqrt{(L+x)^2+(L-y)^2+z^2}} \right) \\
 &+ \frac{\mu_0 I(t)(L-x)}{4\pi(L-x)^2+z^2} \left(\frac{L+y}{\sqrt{(L-x)^2+(L+y)^2+z^2}} + \frac{L-y}{\sqrt{(L-x)^2+(L-y)^2+z^2}} \right) \\
 &+ \frac{\mu_0 I(t)(L+x)}{4\pi(L+x)^2+z^2} \left(\frac{L-y}{\sqrt{(L+x)^2+(L-y)^2+z^2}} + \frac{L+y}{\sqrt{(L+x)^2+(L+y)^2+z^2}} \right)
 \end{aligned} \tag{1}$$

where μ_0 is the magnetic conductivity in the vacuum, $I(t)$ is the transmitting current at the moment t , the transmitting antenna is $2L$ long, and x , y and z are space coordinates. The distribution graph of the primary magnetic field that is vertical to the x -coordinate of the transmitting plane at the moment t is shown in Figure 3.

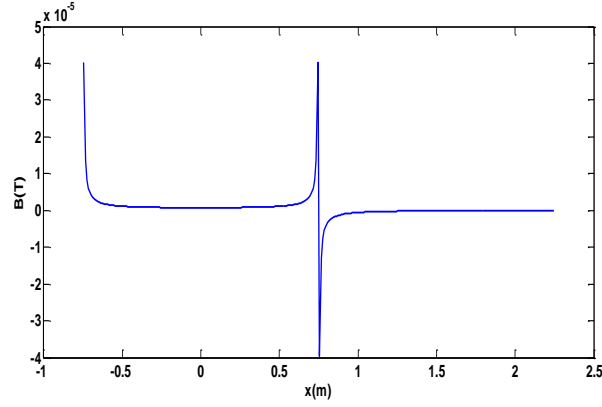


Fig.3. Distribution Graph of the Primary Magnetic Field That Is Vertical to The X-Coordinate of the Transmitting Plane

Assuming that the coordinate of the central point of the receiving antenna is $(x_0, 0, z)$, and the magnetic flux of the vertical primary magnetic field $\phi_{R1}(x_0, t, z)$ is:

$$\begin{aligned}
& \phi_{R1}(x_0, t, z) \\
&= \int_{-L}^L \int_{x_0-L}^{x_0+L} \frac{\mu_0 I(t)(L+y)}{4\pi(L+y)^2+z^2} \left(\frac{L+x}{\sqrt{(L+x)^2+(L+y)^2+z^2}} + \frac{L-x}{\sqrt{(L-x)^2+(L+y)^2+z^2}} \right) dx dy \\
&+ \int_{-L}^L \int_{x_0-L}^{x_0+L} \frac{\mu_0 I(t)(L-y)}{4\pi(L-y)^2+z^2} \left(\frac{L-x}{\sqrt{(L-x)^2+(L-y)^2+z^2}} + \frac{L+x}{\sqrt{(L+x)^2+(L-y)^2+z^2}} \right) dx dy \\
&+ \int_{-L}^L \int_{x_0-L}^{x_0+L} \frac{\mu_0 I(t)(L-x)}{4\pi(L-x)^2+z^2} \left(\frac{L+y}{\sqrt{(L-x)^2+(L+y)^2+z^2}} + \frac{L-y}{\sqrt{(L-x)^2+(L-y)^2+z^2}} \right) dx dy \\
&+ \int_{-L}^L \int_{x_0-L}^{x_0+L} \frac{\mu_0 I(t)(L+x)}{4\pi(L+x)^2+z^2} \left(\frac{L-y}{\sqrt{(L+x)^2+(L-y)^2+z^2}} + \frac{L+y}{\sqrt{(L+x)^2+(L+y)^2+z^2}} \right) dx dy
\end{aligned} \tag{2}$$

We use $F_1(x_0, t, z)$, $F_2(x_0, t, z)$, $F_3(x_0, t, z)$ and $F_4(x_0, t, z)$ to represent the above four items in formula (2).

$$\begin{aligned}
& F_1(x_0, t, z) \\
&= \frac{\mu_0 I(t)}{4\pi} \int_{-L}^L \frac{(L+y)}{(L+y)^2+z^2} dy \int_{x_0-L}^{x_0+L} \frac{L+x}{\sqrt{(L+x)^2+(L+y)^2+z^2}} dx \\
&+ \frac{\mu_0 I(t)}{4\pi} \int_{-L}^L \frac{(L+y)}{(L+y)^2+z^2} dy \int_{x_0-L}^{x_0+L} \frac{L-x}{\sqrt{(L-x)^2+(L+y)^2+z^2}} dx
\end{aligned} \tag{3}$$

We calculate the integration of x in the first item in formula (3):

$$\begin{aligned}
& \int_{x_0-L}^{x_0+L} \frac{L+x}{\sqrt{(L+x)^2 + (L+y)^2 + z^2}} dx \\
&= \sqrt{(L+x)^2 + (L+y)^2 + z^2} \Big|_{x_0-L}^{x_0+L} \\
&= \sqrt{(x_0+2L)^2 + (L+y)^2 + z^2} - \sqrt{x_0^2 + (L+y)^2 + z^2}
\end{aligned} \tag{4}$$

Similarly, the integration of x in the second item in formula (3) is:

$$\begin{aligned}
& \int_{x_0-L}^{x_0+L} \frac{L-x}{\sqrt{(L-x)^2 + (L+y)^2 + z^2}} dx \\
&= -\sqrt{(L-x)^2 + (L+y)^2 + z^2} \Big|_{x_0-L}^{x_0+L} \\
&= \sqrt{(x_0-2L)^2 + (L+y)^2 + z^2} - \sqrt{x_0^2 + (L+y)^2 + z^2}
\end{aligned} \tag{5}$$

The formulas (4) and (5) are substituted into formula (3), and we have:

$$\begin{aligned}
& F_1(x_0, t, z) \\
&= \frac{\mu_0 I(t)}{4\pi} \int_{-L}^L \frac{(L+y)}{(L+y)^2 + z^2} \sqrt{(x_0+2L)^2 + (L+y)^2 + z^2} dy \\
&+ \frac{\mu_0 I(t)}{4\pi} \int_{-L}^L \frac{(L+y)}{(L+y)^2 + z^2} \sqrt{(x_0-2L)^2 + (L+y)^2 + z^2} dy \\
&- \frac{\mu_0 I(t)}{2\pi} \int_{-L}^L \frac{(L+y)}{(L+y)^2 + z^2} \sqrt{x_0^2 + (L+y)^2 + z^2} dy
\end{aligned} \tag{6}$$

Let

$$A = \sqrt{(x_0+2L)^2 + (L+y)^2 + z^2} \tag{7}$$

and we have

$$dA = \frac{L+y}{\sqrt{(x_0+2L)^2 + (L+y)^2 + z^2}} dy \tag{8}$$

$$(L+y)^2 + z^2 = A^2 - (x_0+2L)^2 \tag{9}$$

The formulas (8) and (9) are substituted into formula (6), and thus the first item in formula (6) is:

$$\begin{aligned}
& F_{11}(x_0, t, z) \\
&= \frac{\mu_{\sigma} I(t)}{4\pi} \int_{-L}^L \frac{(L+y)}{(L+y)^2+z^2} \sqrt{(x_0+2L)^2+(L+y)^2+z^2} dy \\
&= \frac{\mu_{\sigma} I(t)}{4\pi} \int_{\sqrt{(x_0+2L)^2+z^2}}^{\sqrt{(x_0+2L)^2+4L^2+z^2}} \frac{A^2}{A^2-(x_0+2L)^2} dA \\
&= \frac{\mu_{\sigma} I(t)}{4\pi} \int_{\sqrt{(x_0+2L)^2+z^2}}^{\sqrt{(x_0+2L)^2+4L^2+z^2}} 1 + \frac{(x_0+2L)^2}{A^2-(x_0+2L)^2} dA \\
&= \frac{\mu_{\sigma} I(t)}{4\pi} \int_{\sqrt{(x_0+2L)^2+z^2}}^{\sqrt{(x_0+2L)^2+4L^2+z^2}} 1 + \frac{x_0+2L}{2} \left(\frac{1}{A-(x_0+2L)} - \frac{1}{A+(x_0+2L)} \right) dA \\
&= \frac{\mu_{\sigma} I(t)}{4\pi} \left(\sqrt{(x_0+2L)^2+4L^2+z^2} - \sqrt{(x_0+2L)^2+z^2} \right) \\
&+ \frac{\mu_{\sigma} I(t)(x_0+2L)}{8\pi} \ln \left(\frac{\sqrt{(x_0+2L)^2+4L^2+z^2} - (x_0+2L)}{\sqrt{(x_0+2L)^2+4L^2+z^2} + (x_0+2L)} \right) \\
&+ \frac{\mu_{\sigma} I(t)(x_0+2L)}{8\pi} \ln \left(\frac{\sqrt{(x_0+2L)^2+z^2} + (x_0+2L)}{\sqrt{(x_0+2L)^2+z^2} - (x_0+2L)} \right)
\end{aligned} \tag{10}$$

Similarly, the second and third items in formula (6) are:

$$\begin{aligned}
& \frac{\mu_{\sigma} I(t)}{4\pi} \int_{-L}^L \frac{(L+y)}{(L+y)^2+z^2} \sqrt{(x_0-2L)^2+(L+y)^2+z^2} dy \\
&= \frac{\mu_{\sigma} I(t)}{4\pi} \left(\sqrt{(x_0-2L)^2+4L^2+z^2} - \sqrt{(x_0-2L)^2+z^2} \right) \\
&+ \frac{\mu_{\sigma} I(t)(x_0-2L)}{8\pi} \ln \left(\frac{\sqrt{(x_0-2L)^2+4L^2+z^2} - (x_0-2L)}{\sqrt{(x_0-2L)^2+4L^2+z^2} + (x_0-2L)} \right) \\
&+ \frac{\mu_{\sigma} I(t)(x_0-2L)}{8\pi} \ln \left(\frac{\sqrt{(x_0-2L)^2+z^2} + (x_0-2L)}{\sqrt{(x_0-2L)^2+z^2} - (x_0-2L)} \right)
\end{aligned} \tag{11}$$

$$\begin{aligned}
& - \frac{\mu_{\sigma} I(t)}{2\pi} \int_{-L}^L \frac{(L+y)}{(L+y)^2+z^2} \sqrt{x_0^2+(L+y)^2+z^2} dy \\
&= - \frac{\mu_{\sigma} I(t)}{2\pi} \left(\sqrt{x_0^2+4L^2+z^2} - \sqrt{x_0^2+z^2} \right) \\
&- \frac{\mu_{\sigma} I(t)x_0}{4\pi} \ln \left(\frac{\left(\sqrt{x_0^2+4L^2+z^2} - x_0 \right) \left(\sqrt{x_0^2+z^2} + x_0 \right)}{\left(\sqrt{x_0^2+4L^2+z^2} + x_0 \right) \left(\sqrt{x_0^2+z^2} - x_0 \right)} \right)
\end{aligned} \tag{12}$$

For $F_2(x_0, t, z)$, let

$$y = -m \tag{13}$$

and we have

$$\begin{aligned}
& E_2(x_0, t, z) \\
&= \int_{-L}^L \int_{x_0-L}^{x_0+L} \frac{\mu_0 I(t)(L+m)}{4\pi(L+m)^2+z^2} \left(\frac{L-x}{\sqrt{(L-x)^2+(L+m)^2+z^2}} \right) dx dm \\
&+ \int_{-L}^L \int_{x_0-L}^{x_0+L} \frac{\mu_0 I(t)(L+m)}{4\pi(L+m)^2+z^2} \left(\frac{L+x}{\sqrt{(L+x)^2+(L+m)^2+z^2}} \right) dx dm \\
&= E_1(x_0, t)
\end{aligned} \tag{14}$$

For $F_3(x_0, t, z)$:

$$\begin{aligned}
& F_3(x_0, t, z) \\
&= \frac{\mu_0 I(t)}{4\pi} \int_{x_0-L}^{x_0+L} \frac{(L-x)}{(L-x)^2+z^2} dx \int_{-L}^L \frac{L+y}{\sqrt{(L-x)^2+(L+y)^2+z^2}} dy \\
&+ \frac{\mu_0 I(t)}{4\pi} \int_{x_0-L}^{x_0+L} \frac{(L-x)}{(L-x)^2+z^2} dx \int_{-L}^L \frac{L-y}{\sqrt{(L-x)^2+(L-y)^2+z^2}} dy
\end{aligned} \tag{15}$$

We calculate the integration of y in the first item in formula (15):

$$\begin{aligned}
& \int_{-L}^L \frac{L+y}{\sqrt{(L-x)^2+(L+y)^2+z^2}} dy \\
&= \sqrt{(L-x)^2+(L+y)^2+z^2} \Big|_{-L}^L \\
&= \sqrt{(L-x)^2+4L^2+z^2} - \sqrt{(L-x)^2+z^2}
\end{aligned} \tag{16}$$

Similarly, the integration of y in the second item in formula (15) is:

$$\begin{aligned}
& \int_{-L}^L \frac{L-y}{\sqrt{(L-x)^2+(L-y)^2+z^2}} dy \\
&= -\sqrt{(L-x)^2+(L-y)^2+z^2} \Big|_{-L}^L \\
&= \sqrt{(L-x)^2+4L^2+z^2} - \sqrt{(L-x)^2+z^2}
\end{aligned} \tag{17}$$

The formulas (16) and (17) are substituted into formula (15), and we have:

$$\begin{aligned}
& F_3(x_0, t, z) \\
&= \frac{\mu_0 I(t)}{2\pi} \int_{x_0-L}^{x_0+L} \frac{(L-x)}{(L-x)^2+z^2} \sqrt{(L-x)^2+4L^2+z^2} dx \\
&- \frac{\mu_0 I(t)}{2\pi} \int_{x_0-L}^{x_0+L} \frac{(L-x)}{(L-x)^2+z^2} \sqrt{(L-x)^2+z^2} dx
\end{aligned} \tag{18}$$

Similar to formulas (10) and (11), the first item in formula (18) is:

$$\begin{aligned}
& \frac{\mu_0 I(t)}{2\pi} \int_{x_0-L}^{x_0+L} \frac{(L-x)}{(L-x)^2+z^2} \sqrt{(L-x)^2+4L^2+z^2} dx \\
&= \frac{\mu_0 I(t)}{2\pi} \left(\sqrt{(x_0-2L)^2+4L^2+z^2} - \sqrt{4L^2+x_0^2+z^2} \right) \\
&+ \frac{\mu_0 I(t)}{2\pi} L \ln \left(\frac{\left(\sqrt{(x_0-2L)^2+4L^2+z^2} - 2L \right) \left(\sqrt{x_0^2+4L^2+z^2} + 2L \right)}{\left(\sqrt{(x_0-2L)^2+4L^2+z^2} + 2L \right) \left(\sqrt{x_0^2+4L^2+z^2} - 2L \right)} \right)
\end{aligned} \tag{19}$$

the second item in formula (18) is:

$$\begin{aligned}
& - \frac{\mu_0 I(t)}{2\pi} \int_{x_0-L}^{x_0+L} \frac{(L-x)}{(L-x)^2+z^2} \sqrt{(L-x)^2+z^2} dx \\
&= - \frac{\mu_0 I(t)}{2\pi} \int_{x_0-L}^{x_0+L} \frac{(L-x)}{\sqrt{(L-x)^2+z^2}} dx \\
&= \frac{\mu_0 I(t)}{2\pi} \sqrt{(L-x)^2+z^2} \Big|_{x_0-L}^{x_0+L} \\
&= \frac{\mu_0 I(t)}{2\pi} \left(\sqrt{x_0^2+z^2} - \sqrt{(2L-x_0)^2+z^2} \right)
\end{aligned} \tag{20}$$

In the similar way, for $F_4(x_0, t)$:

$$\begin{aligned}
& F_4(x_0, t, z) \\
&= \frac{\mu_0 I(t)}{4\pi} \int_{x_0-L}^{x_0+L} \frac{(L+x)}{(L+x)^2+z^2} dx \int_{-L}^L \frac{L-y}{\sqrt{(L+x)^2+(L-y)^2+z^2}} dy \\
&+ \frac{\mu_0 I(t)}{4\pi} \int_{x_0-L}^{x_0+L} \frac{(L+x)}{(L+x)^2+z^2} dx \int_{-L}^L \frac{L+y}{\sqrt{(L+x)^2+(L+y)^2+z^2}} dy
\end{aligned} \tag{21}$$

We calculate the integration of y in the first item in formula (21):

$$\begin{aligned}
& \int_{-L}^L \frac{L-y}{\sqrt{(L+x)^2 + (L-y)^2 + z^2}} dy \\
&= -\sqrt{(L+x)^2 + (L-y)^2 + z^2} \Big|_{-L}^L \\
&= \sqrt{(L+x)^2 + 4L^2 + z^2} - \sqrt{(L+x)^2 + z^2}
\end{aligned} \tag{22}$$

Similarly, the integration of y in the second item in formula (21) is:

$$\begin{aligned}
& \int_{-L}^L \frac{L+y}{\sqrt{(L+x)^2 + (L+y)^2 + z^2}} dy \\
&= \sqrt{(L+x)^2 + (L+y)^2 + z^2} \Big|_{-L}^L \\
&= \sqrt{(L+x)^2 + 4L^2 + z^2} - \sqrt{(L+x)^2 + z^2}
\end{aligned} \tag{23}$$

The formulas (22) and (23) are substituted into formula (21), and we have:

$$\begin{aligned}
& F_4(x_0, t, z) \\
&= \frac{\mu_0 I(t)}{2\pi} \int_{x_0-L}^{x_0+L} \frac{(L+x)}{(L+x)^2 + z^2} \sqrt{(L+x)^2 + 4L^2 + z^2} dx \\
&- \frac{\mu_0 I(t)}{2\pi} \int_{x_0-L}^{x_0+L} \frac{(L+x)}{(L+x)^2 + z^2} \sqrt{(L+x)^2 + z^2} dx
\end{aligned} \tag{24}$$

Similar to formulas (10) and (11), the first item in formula (24) is:

$$\begin{aligned}
& \frac{\mu_0 I(t)}{2\pi} \int_{x_0-L}^{x_0+L} \frac{(L+x)}{(L+x)^2 + z^2} \sqrt{(L+x)^2 + 4L^2 + z^2} dx \\
&= \frac{\mu_0 I(t)}{2\pi} \left(\sqrt{(x_0+2L)^2 + 4L^2 + z^2} - \sqrt{4L^2 + x_0^2 + z^2} \right) \\
&+ \frac{\mu_0 I(t)}{2\pi} L \ln \left(\frac{\sqrt{(x_0+2L)^2 + 4L^2 + z^2} - 2L \sqrt{x_0^2 + 4L^2 + z^2} + 2L}{\sqrt{(x_0+2L)^2 + 4L^2 + z^2} + 2L \sqrt{x_0^2 + 4L^2 + z^2} - 2L} \right)
\end{aligned} \tag{25}$$

The second item in formula (24) is:

$$\begin{aligned}
& - \frac{\mu_0 I(t)}{2\pi} \int_{x_0-L}^{x_0+L} \frac{(L+x)}{(L+x)^2 + z^2} \sqrt{(L+x)^2 + z^2} dx \\
&= - \frac{\mu_0 I(t)}{2\pi} \int_{x_0-L}^{x_0+L} \frac{(L+x)}{\sqrt{(L+x)^2 + z^2}} dx \\
&= - \frac{\mu_0 I(t)}{2\pi} \sqrt{(L+x)^2 + z^2} \Big|_{x_0-L}^{x_0+L} \\
&= \frac{\mu_0 I(t)}{2\pi} \left(\sqrt{x_0^2 + z^2} - \sqrt{(2L+x_0)^2 + z^2} \right)
\end{aligned} \tag{26}$$

According to formula (2), only by calculating the appropriate value of x_0 can the kernel function be normalized:

$$F(x_0) = \frac{4\pi\phi_{R1}(x_0, t)}{\mu I(t)} = 0 \quad (27)$$

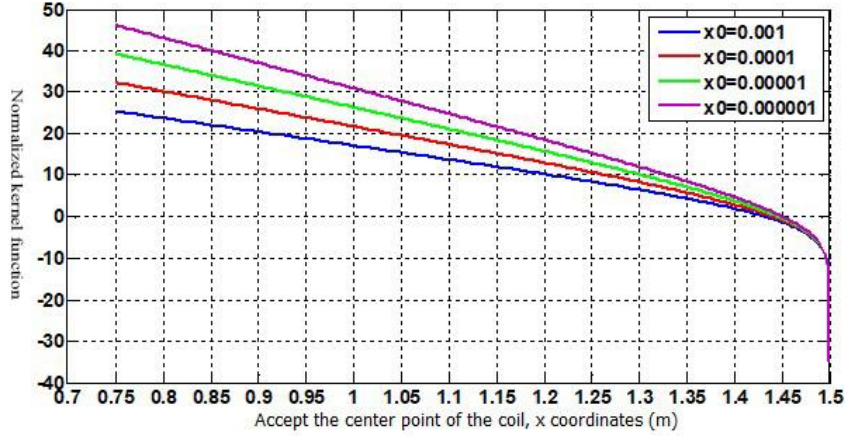


Fig.4. The Curve of The Normalized Kernel Function

When $z=0$, there are extremums in the rhombic edge, which means that the curve in Figure 4 is plotted at different z values. Figure 4 shows that the kernel function is monotonically decreasing curve.

$$F(x_0) \approx 0, x_0 \approx 1.451 \quad (28)$$

Let

$$x_0 = L + KL \quad (29)$$

where K is the coefficient of the position. By substituting formula (31) into formula (29), it can be testified that for any L value, we have

$$F(K) \approx 0, K \approx 0.93 \quad (30)$$

4. The Measured Attenuation Curve

(1) Indoor comparison experiments

In order to verify the advanced nature of the staggered arrangement of the transmitting and receiving antennas, the YCS1024 intrinsic-safe mining transient electro magnetometer is used in the laboratory to measure shallow-area low resistivity anomalies. The measured values in the cases of overlapping loop and staggered antennas are compared. To verify the anomaly detection effect and the primary field effect in the two cases, we locate the artificial low resistivity in the center of the staggered antenna, as shown in Figure 1. To highlight the primary field effect, we use bare bridge as the transmitting bridge with the support of the shut-off acceleration technology. The test parameters are listed in Table 1:

Tab.1. Test Parameters

| | |
|---|-------|
| Transmitting current | 3.9A |
| Shut-off time | 180μs |
| transmitting antenna length | 1.5m |
| transmitting antenna turns | 10za |
| Receiving antenna length | 1.5m |
| Receiving antenna turns | 20za |
| Position coefficient of the staggered transmitting and receiving antennas | 0.93 |

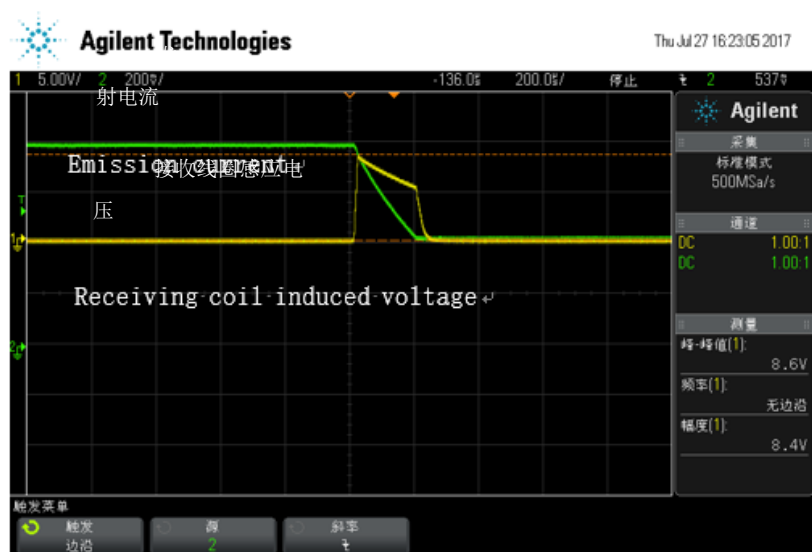


Fig.5. The Waveform of the Transmitting Current and The Induced Voltage of The Receiving Coil in The Case of Overlapping Loop

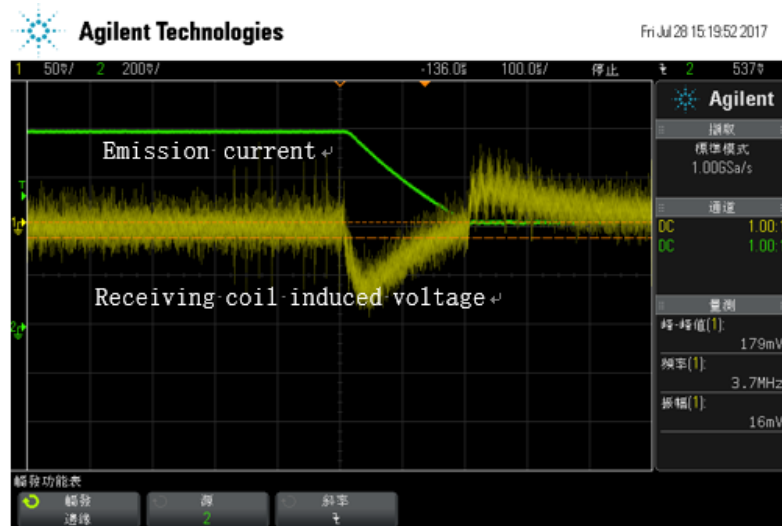


Fig.6. The Waveform of the Transmitting Current and The Induced Voltage of The Receiving Coil in the Case of Staggered Loops

Figure 5 and Figure 6 are the waveform of the transmitting current and the induced voltage of the receiving coil in the cases of overlapping loop and staggered loops, respectively. As can be seen from Figure 5, under the shut-off effect, the total field is composed of the primary field and the secondary field. As the primary field dominates the total field, the total field is positive from the beginning of the shut-off to a short time after the end of the shut-off. As can be seen in Figure 6, as the magnetic flux in the inner primary field of the receiving coil is 0, there is barely any shut-off effect, which means that the dominant role is played by the secondary field that is produced from low-resistivity anomaly in the shut-off period. As the low resistivity anomaly happens between the receiving and transmitting coils, the total field is negative; in a short time after the end of the shut-off, as the secondary field continues to dominate the total field, the total field is positive.

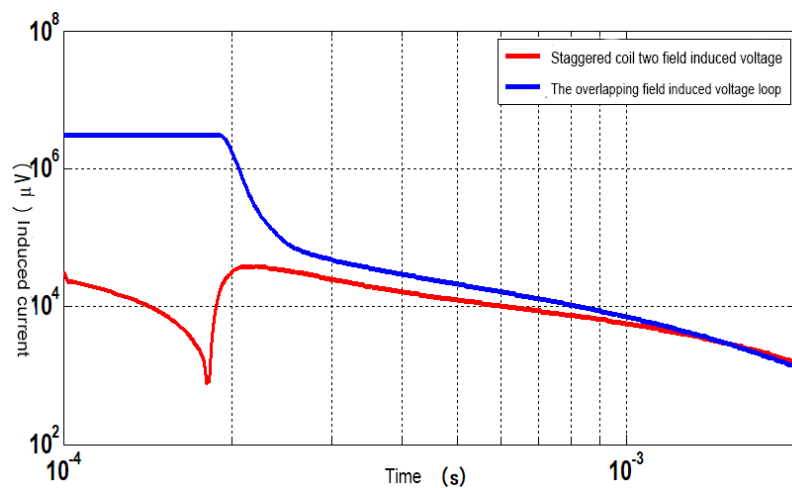


Fig.7. Comparison of Attenuation Curves

Figure 7 shows the comparison of the attenuation curves of induced voltage between the total field in the case of overlapping loop and the secondary field in the case of staggered loop. T1 is the moment of complete shut-off of the transmitting current; TCROS is the time of the secondary field transiting from negative to positive in the case of staggered loop; TOVER is the time of the shut-off effect in the case of overlapping loop. It can be seen from the figure that TCROS is about 30 μ s and TOVER is about 120 μ s. This means that the Tover is about 4 times that of TCROS.

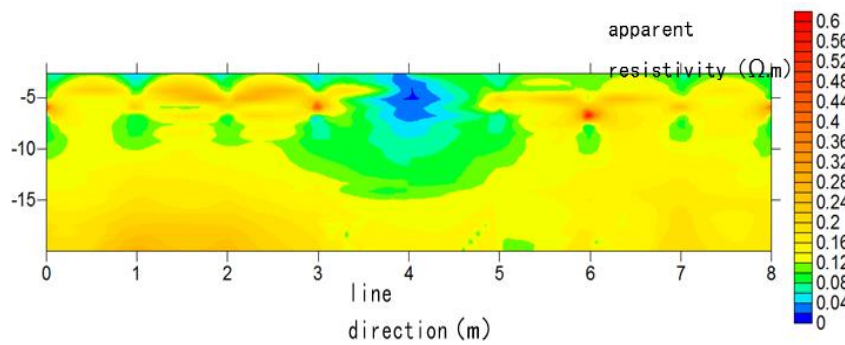


Fig.8. The Profile of the Apparent Resistivity in the Case of Staggered Loop

Figure 8 is the profile of the apparent resistivity in detecting the low resistivity anomaly by using staggered loop. The explanatory power of apparent resistivity is effective upon the elimination of the shut-off effect. As can be seen from Figure 8, the staggered loop can help accurately detect low resistivity anomaly. As it offsets the effect of primary field in the shut-off period, the apparent resistivity can detect low resistivity anomalies after the complete shut-off.

(2) on-spot detection

In order to verify the accuracy of staggered loop detection on low resistivity anomaly in shallow area, we conduct a field survey on the water-enriched roadway in the Chayuan Coal Mine in Dazhou city, Sichuan province. Figure 9 is the profile of the measured apparent resistivity in the case of staggered loop. Table 2 is the detection parameters.

Tab.2. Test Parameter Table

| | |
|----------------------------|--|
| Instrument | YCS10 explosion-proof and intrinsically-safe mining transient electro magnetometer |
| attitude angle measurement | YHZ180/180 intrinsically-safe mining attitude angle measuring instrument |
| Transmitting current | 10A |

| | |
|---|------------|
| Shut-off time | 92 μ s |
| transmitting antenna length | 1.5m |
| transmitting antenna turns | 10za |
| Receiving antenna length | 1.5m |
| Receiving antenna turns | 20za |
| Position coefficient of the staggered transmitting and receiving antennas | 0.93 |

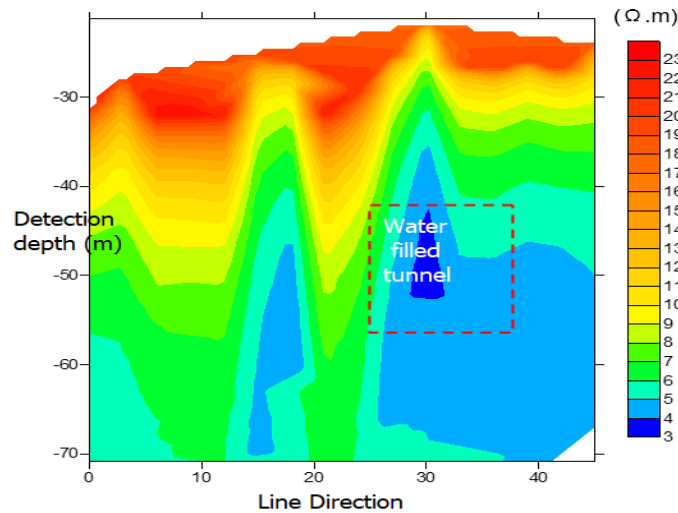


Fig.9. The Profile of the Measured Apparent Resistivity at 10 Degrees Downward the + 76 Winch Track

It can be seen from Figure 9, due to the use of the staggered loop detection, a low resistivity anomaly occurs in the area that is 30m in the detection direction, 32m deep, and 10 degrees downward, after the shut-off effect is eliminated. According to geological data, this area should be a water-filled roadway. The on-spot drilling result shows that there is water in the area that is 30m in the detection direction, 10 degrees downward, and 35m deep, which agrees with the detection test and the geological data. Therefore, the staggered loop detection method is proved effective.

Conclusion

(1) An analysis is conducted on the distribution of the primary field in and out of the transmitting coil as well as its influence on the secondary field after current shut-off. Based on the analysis result, we put forward the method of staggered arrangement of receiving and transmitting antennas to counteract the primary field.

(2) The analytical expression of the magnetic flux in the primary field is deduced in the interior of the receiving antenna; then, the position coefficient of the receiving coil is calculated as 0.93 or so when the magnetic flux is 0.

(3) Through the attenuation curve and apparent resistivity profile of the detected ground-level low resistivity anomaly in the lab, it is proved that due to the offsetting of the primary field, the time of shut-off effect is shorter with staggered loop than with overlapping loop, and the staggered loop can detect shallow-area low resistivity anomaly early after the end of shut-off.

(4) Through the field detection of water-filled roadway, the staggered loop is proved effective in detecting low resistivity anomalies.

Acknowledgments

The project is supported by National Science and Technology Major Project of the Ministry of Science and Technology of China (Grant No. 2016ZX05045-002-0003 and 2016ZX05045004-007).

References

1. J. Lin, L. Wang, X. Wang, M. Cao, L. Fu, X. Shang, Research and development on the air-core coil sensor for mine transient electromagnetic exploration, 2016, Chinese Journal of Geophysics, vol. 59, no. 2, pp. 721-730.
2. J.L. Cheng, D. Chen, G.Q. Xue, H. Qiu, X.T. Zhou, Synthetic aperture imaging in advanced detection of roadway using the mine transient electromagnetic method, 2016, Chinese Journal of Geophysics, vol. 59, no. 2, pp. 731-738.
3. D.H. Bai, M. Maxwell, The effect of two types of turn-off current on tem responses and the correction techniques, 2001, Seismology and Geology, vol. 23, no. 2, pp. 245-251.
4. Y.J. Ji, J. Lin, Z. Wang, S.B. Yu, J. Wang, Analysis of distortion in all-time transient electromagnetic field based on inducing of ramp switch-off current for shallow survey, 2007, Chinese Journal of Radio Science, vol. 22, no. 2, pp. 316-320.
5. Y.J. Ji, J. Lin, Z. Wang, Analysis and numerical removing of distortion in transient electromagnetic receiver device for shallow sounding, 2007, Progress in Geophysics. vol. 22, no. 2, pp. 316-320.
6. Z.X. Liu, J.W. Wu, Theoretical research and application of blind area problem on mine transient electromagnetic method, 2011, The 10th China International Geo-Electromagnetic Workshop 2011, pp. 284-286.

7. S.L. Wang, Y.Z. Wang, Y.Y. Sui, Q. Wang, J. Lin, A bird calibration device of Helicopter-borne TEM with concentric bucking loop, 2011, Chinese Journal Geophys, vol. 54, no. 9, pp. 2397-2406.
8. M. Svllans, Quantitative interpretation of responses of Heliecopter-borne coneentric loop EM geophysical survey systems [Bachelor of Science], 2006.Ottawa, Ontario: Carleton University Earth Sciences.
9. S.J. Baleh, W.P. Boyko, N.R. Paterson, The AeroTEM airborne electromagnetic system, 2003, The Leading Edge, vol. 22, no. 6, pp. 562-566.
10. Y.C. Xu, J. Lin, S.Y. Li, X.S. Zhang, Y. Wang, Calculation of full-waveform airborne electromagnetic response with three-dimension finite-difference solution in time-domain, 2012, Chinese Journal Geophys, vol. 55, no. 6, pp. 2105-2114.
11. Z.L. Jiang, J.C. Yu, W.T. Sun, Study on mine transient electromagnetic method affected to full space response of low resistance body, 2012, Coal science and technology, vol. 40, no. 8, pp. 107-110.
12. Z.H. Jiang, J.H. Yue, S.C. Liu, Mine transient electromagnetic observation system of small multi-turn coincident configuration, 2007, Journal of China Coal Society, vol. 32, no. 11, pp. 1152-1156.